14th Australasian Fluid Mechanics Conference
Adelaide University, Adelaide, Australia
10-14 December 2001

A Mechanism for Jet Precession in Axisymmetric Sudden Expansions

R.M. Kelso

Department of Mechanical Engineering
Adelaide University, South Australia, 5005 AUSTRALIA

Abstract

A new model describes the flow pattern within a fluidic precessing jet chamber. The model offers a simple explanation of the precessing jet flow and the mechanism which produces the precession. The model is used to derive an equation relating the Strouhal number of precession to the chamber geometry.

Introduction

Background

The fluidic precessing jet (FPJ) was invented in 1988 G. J. Nathan and R. E. Luxton after several years of searching for a more efficient and clean combustion device. With the long-term partnership of an Adelaide company, Fuel and Combustion Technology Pty Ltd., the inventors developed the FPJ into an industrial scale burner known as the GyroTherm. So far more than 20 GyroTherm burners with capacities to 100 MW have been installed world-wide. The most noticeable of these was the main flame at the Sydney 2000 Olympic Games.

The process of industrialization of the FPJ has been achieved mainly through the understanding of the characteristics of the precessing jet outside the chamber and the effect of the chamber geometry on the precession characteristics. Some additional features such as the exit lip and the centre-body have improved the performance of the device in its burner application. Interestingly, the flow pattern inside the chamber and the mechanism by which the jet precesses have remained only partially understood as will be shown in the following section. The most comprehensive explanation of the mechanism of precession is provided by Nathan, Hill & Luxton [5], from which much information has been drawn in this paper. It is the author's view that if the precessing jet flow is to be modelled, optimised and applied to applications other than gas-fired burners, then the mechanism which produces precession must be understood in detail. The present paper is based on a more extensive and detailed discussion provided in Kelso [3].

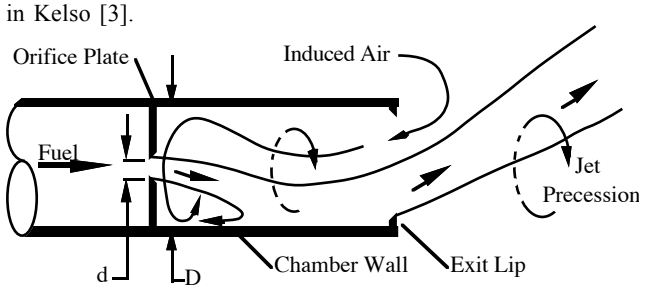

Figure 1. Schematic representation of the precessing jet flow.

The geometry of the precessing jet is shown in Figure 1. The flow from a straight pipe, contraction or orifice plate (diameter d) enters a chamber through an axisymmetric expansion (diameter D) and reattaches asymmetrically to the side wall of the chamber. A fluidic instability causes the reattaching jet to precess around the inside wall of the chamber, thus producing a precessing external jet flow. The deflection and precession together generate an unusual flow field beyond the chamber exit. This flow is characterized by a high rate of decay of the centreline mean velocity, a high turbulence intensity and large energetic vortex structures. More details can be found in [2,4,5,7].

Previous Models

Significant understanding of the flow within the chamber was achieved by Nathan [5], who used several different techniques to determine that the flow attached asymmetrically on the chamber wall. He suggested that the jet precession is due to a positive feedback mechanism. Nathan, Hill & Luxton [4] later conducted detailed flow visualization experiments. These included particle-streak visualization in water, which clearly showed the jet attached to the side of the chamber and precessing azimuthally. Instantaneous images also showed that some of the jet fluid recirculates back upstream towards the base of the chamber. Time-averaged surface flow patterns were obtained using the china clay method in air and interpreted using flow topology concepts. The patterns, shown schematically in Figure 2, identify significant features in the time-averaged surface flow. These include a spiral-like entrainment pattern of fluid at the base of the chamber and three bifurcation lines on the wall of the chamber. The central positive bifurcation line (PB) on the side of the chamber corresponds well with the reattachment location observed in the water model. The negative bifurcation line (NB) on the chamber wall near the base was interpreted in [5] as being due to a flow feature on the side opposite the jet attachment. The negative bifurcation adjacent to the exit is likely to be brought about by the local effect of the lip itself.

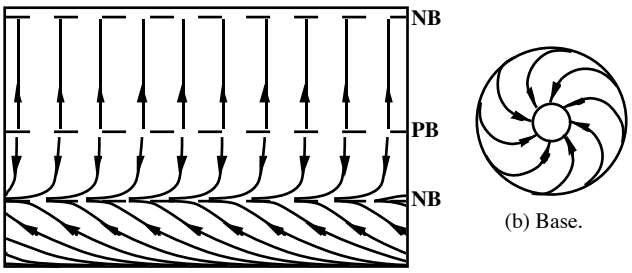

(a) Internal surface of chamber.

Figure 2. Schematic representations of the time-averaged surface streaklines formed on the inside of the FPJ chamber. (a) Internal surface of the chamber opened out flat. The direction of the jet is from bottom to top. (b) Base of the chamber (orifice plate) as seen from the chamber exit. NB = negative bifurcation, PB = positive bifurcation. The original images can be found in Nathan, Hill & Luxton [5].

On the basis of these observations and a number of others in [5], a simple description of the flow was proposed, as shown in Figure 1. Although descriptive of the general appearance of the flow and the pathlines occurring therein, the model offers no physical mechanism for the precession.

Another interesting result is shown in Wong *et al.* [7] where the velocity decay of the jet within the FPJ chamber is compared with that of a jet in counter-flow. The agreement is relatively strong, which suggests that the model has some merit, but it still does not explain precession.

The New Interpretation of the Mechanism

Steady Reattachment

The new model began firstly as an analysis of the streamline pattern and vortex line evolution associated with the steady reattachment of the jet to the chamber wall. A schematic diagram of this process is shown in Figure 3. The reader is referred to Kelso [3] for the inferred surface and cross-sectional streamline patterns. The main features of the attachment region are similar to the well-established "U-shaped separation" pattern described in Perry & Chong [6]. Although the main features of the flow pattern are known to exist in reattaching jets, many of the features in this pattern are inferred using standard topological rules and observations from [4] and [5].

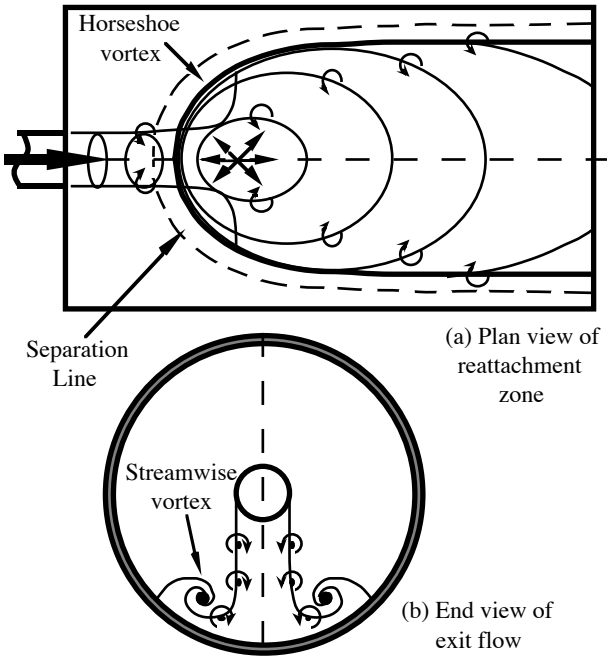

Figure 3. Schematic representation of the stationary rearrachment within the FPJ chamber. Vortex filaments show how the attachment process leads to streamwise vortices in the outflowing jet.

It is concluded that the reattachment causes the jet to roll up into a horse-shoe vortex, with two streamwise "legs". As it rolls up this vortex will entrain induced ambient fluid within the chamber. The entrained flow enters from the chamber's exit opening and flows upstream before turning and becoming entrained into the jet flow. See [3] for details.

Unsteady Reattachment

Once the model for the steady pattern was developed, the response of the pattern to perturbation was investigated. The proposed response is shown in Figure 4. It is first assumed that the jet is displaced sideways at the reattachment point by an infinitesimal amount. This displacement leads to a re-distribution of vorticity in the reattachment zone; the bunching of vortex lines on the side to which the jet is displaced and a spreading of the vortex lines on the opposite side. The bunching of vortex lines will lead to a strong vortex (hence lower pressure) on that side, and the spreading will lead to a large, diffused vortex on the opposite side (higher pressure). This, in-turn, will generate a pressure gradient across the reattachment zone, driving the jet in the direction of the original displacement. This positive feedback process therefore causes the jet and reattachment zone to precess around the chamber wall. The strong vortex ahead of the precessing jet, the “driving vortex”, is likely to convect at a velocity defined by its circulation, core size and distance from the wall.

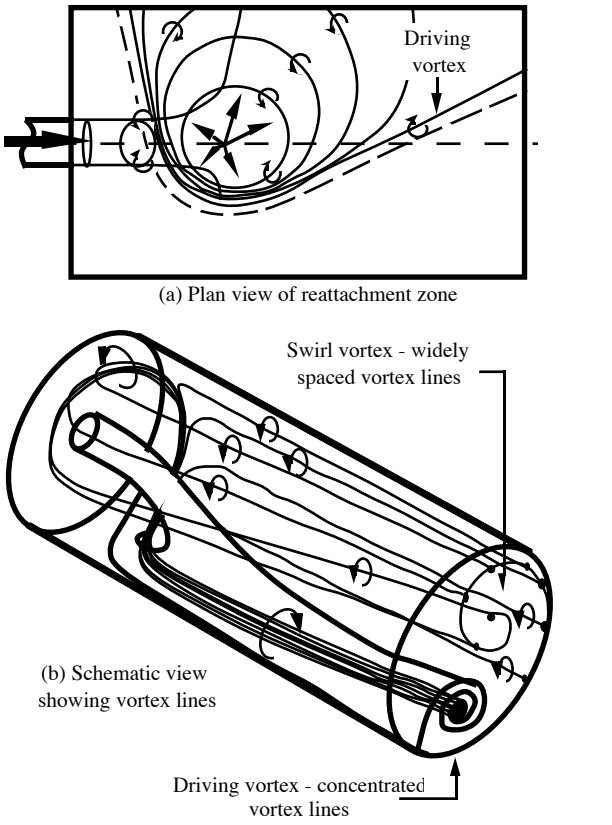

Figure 4. Schematic representation of the precessing jet flow and surrounding flow within the chamber. Vortex lines illustrate how the driving vortex is formed on the leading side of the precessing jet.

Once the pattern is precessing, the horseshoe vortex forms a wide, asymmetric loop as shown in Figure 4. One leg of the loop, the "driving vortex", becomes embedded in the jet which discharges from the chamber. The other leg winds around the chamber base and then into the large, diffuse vortex, the "swirl vortex", in the middle of the chamber. Nathan *et al.* [5] show evidence of this vortex system in Figure 4 of that paper. This process is best illustrated by the vortex lines in Figure 4(b) and the streamline pattern of Figure 5. Although the flow pattern is highly asymmetric, the driving vortex and swirl vortex, being legs of the same horseshoe vortex, must contain identical circulation if the initial jet flow is axisymmetric. In Figure 5(d), the cross-sectional view of the flow is shown. The horseshoe vortex is shown attached to the chamber wall on the jet attachment side, and detached on the opposite side. According to the model, some of the ambient fluid entrained into the chamber will travel towards the low-pressure reattachment region, whereupon it is swept around the base of the chamber, induced by the swirl vortex, before it is entrained into the jet. This explains similar observations by Nathan *et al.* [5].

Comparison with Surface Flow Visualization

The proposed model of the FPJ agrees well with previous observations. Some of these comparisons have been discussed earlier in this paper. The china clay surface flow visualization results presented in [5] are perhaps the most conclusive evidence to date on the FPJ flow pattern. An interpretation of this time-averaged pattern is shown in Figure 2.

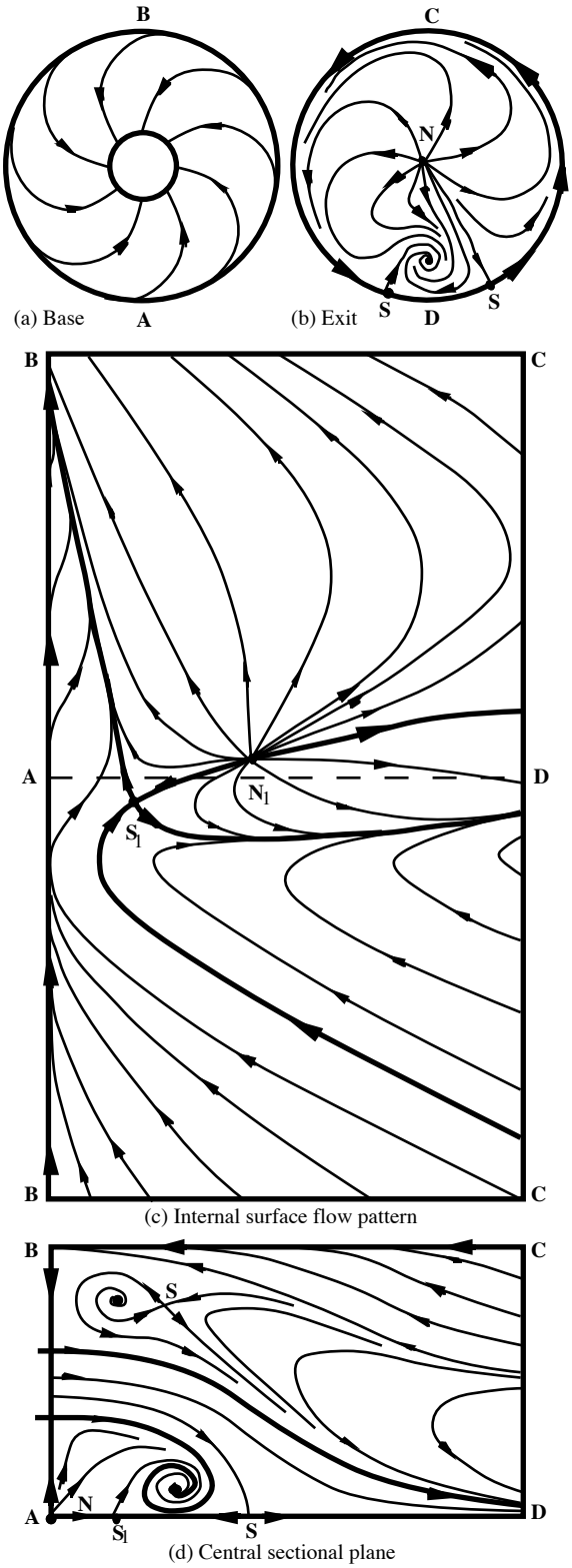

Figure 5. Schematic representation of the unsteady flow pattern within the FPJ chamber when the jet is precessing. In order to see this as a steady pattern the observer is rotating with the same angular velocity as the precessing jet. N = Node, S = Saddle.

Comparison between Figure 2 and the proposed unsteady flow pattern of Figure 5 shows that the central positive bifurcation line (PB) is consistent with the node of attachment of the jet, denoted N_1 in Fig. 5(c). Recognising that the flow velocities in the reattachment region are many times those in other regions of the surface flow (as shown in [7]), the negative bifurcation line near the chamber base could be readily produced by the saddle point (S_1) and the associated reversed flow region between the reattachment point and the chamber base. The surface flow on the chamber base is explained by considering that the asymmetry produced by jet precession will add a tangential component to the otherwise radial flow. The negative bifurcation at the chamber exit is probably the result of the exit lip and is not relevant to the present discussion.

Strouhal Number of Precession

The following analysis defines an appropriate Strouhal number of precession. In the analysis, K_1, K_2, K_3 and K_4 are as yet unknown coefficients. First we assume that the jet impinges on the wall and the jet shear layer vorticiy distorts to form a horse-shoe-shaped attachment region. We estimate that the circulation of the horseshoe vortex scales with the product of the initial velocity difference U across the jet shear layer and the distance turned by the jet, D/2. The constant of proportionality is K_1. Hence,

$$\Gamma_R = \frac{K_1 U D}{2}. \qquad (1)$$

Now assume that all available circulation contributes equally to the formation of the driving vortex and the swirl vortex within the chamber. The motion of the driving vortex is primarily the result of induction by its image in the adjacent wall (see [1]) and by the swirl in the chamber. Induction by other image vortices is assumed negligible. The induction of the driving vortex by its image is depicted in Figure 6. Assuming that the distance between the wall and the vortex core scales with d, we obtain

$$U_c = K_2 \frac{\Gamma_R}{2\pi d}. \qquad (2)$$

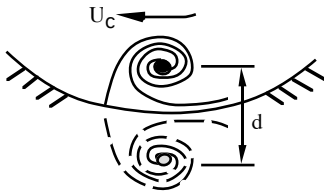

Figure 6. Schematic representation of driving vortex.

The induction of the driving vortex by the swirl is given by

$$U_s = K_3 \frac{\Gamma_R}{\pi D}. \qquad (3)$$

based on the assumption that the distance between the swirling vortex core and the driving vortex scales with D.

The convection speed of the driving vortex will be the difference between the two induced velocities

$$U_d = U_c - U_s = K_2 \frac{\Gamma_R}{2\pi d} - K_3 \frac{\Gamma_R}{\pi D}. \qquad (4)$$

The driving vortex will precess at a mean radius that is less than radius of the chamber. Assuming again that the distance between the wall and the driving vortex core scales with d, we estimate the precession diameter as ($D-K_4 d$). Thus, the precession frequency will be;

$$f = \frac{U_d}{\pi(D - K_4 d)}. \qquad (5)$$

Now define the Strouhal number of precession based on the chamber diameter D and the jet entry velocity U, such that;

$$St_D = \frac{fD}{U}. \qquad (6)$$

Thus, combining equations (1)-(6), we find

$$St_D = \frac{K_1 K_2 \left(\frac{D}{d} - \frac{2K_3}{K_2} \right)}{4\pi^2 \left(1 - K_4 \frac{d}{D} \right)}. \qquad (7)$$

Experimental data from [4] were used to obtain empirical values of the constants in equation (7). This was achieved by a trial-and-error method which minimised the RMS difference between the experimental data and "model" values. The Reynolds number dependence of the Strouhal number prevents a general solution. For a Reynolds number of 100,000, equation (7) becomes

$$St_D = 0.00061 \frac{\left(\frac{D}{d} - 2.3\right)}{\left(1 - 4.6\frac{d}{D}\right)}. \qquad (8)$$

The constant (0.00061) appears to be Reynolds number dependent.

Note that for precession by the proposed mechanism, $U_c > U_s$, and so $D/d > 2K_3/K_2$. Equation 8 shows that $2K_3/K_2 = 2.3$ for the given data. This implies that so long as the expansion ratio is greater than 2.3, then the jet can precess by the proposed mechanism. Constant K_4 is unexpectedly large. This indicates that the model is incomplete or that a larger population of experimental data are required.

The model outlined above is the first published attempt at describing the flow analytically. As yet, the model does not take into account the chamber length and the Reynolds number. These must be included for a general equation to be obtained. The validation of the model and the calculation of the constants require considerably more data than are currently available.

Additional Implications

There are a number of implications that spring from this new model. These are examined and explained in Kelso [3], along with many other ideas.

1. The precession is likely to be highly sensitive to initial conditions such as asymmetries in upstream jet flow. These asymmetries may be expected to cause the jet to attach at one location preferentially and therefore fail to precess. Inlet swirl is likely to bias the direction of precession and increase the strength of the driving vortex. The precession frequency may possibly be varied by controlling the swirl in the jet.
2. Figure 7 describes the vortex system that is likely to be generated by the FPJ nozzle a short time after precession commences. The pattern demonstrates that the model satisfies the condition that vortex lines are closed and circulation is conserved. The precessing jet that leaves the FPJ nozzle will contain predominantly a strong embedded (jet-wise) vortex, rather than a counter-rotating vortex pair. The exit flow angular momentum is likely to be zero (unless vorticity is somehow generated within the chamber or there is swirl in the initial jet).
3. The external flow field will consist of a helically-wound vortex, the sense of which will induce a velocity deficit on the nozzle centreline, and an excess outside the helix, as shown in Figure 7. The overall flow pattern is likely to bear strong similarity to spiral-type vortex breakdown.

Conclusions

A new model for the flow structure and precessional mechanism of the fluidic precessing jet is proposed. Although not yet verified by experiment, the model is strongly anchored to the many observations of the FPJ flow and related reattaching jet flows. An analytical treatment of the model offers a first step towards an equation relating the Strouhal number of precession to the chamber geometry. Comparison with experimental data shows strong agreement. A number of additional implications stem from this work. These will constitute the basis of future research.

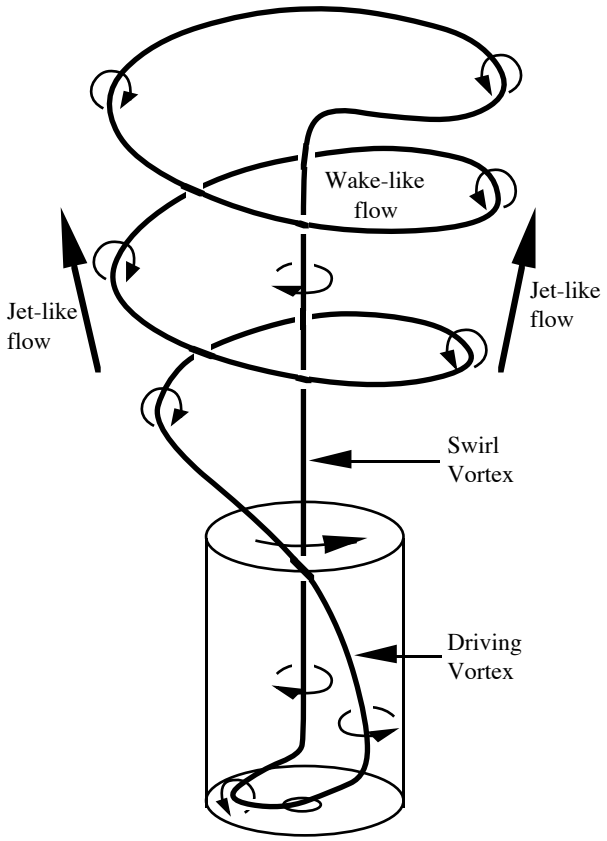

Figure 7. Schematic representation of the vortex system of the FPJ.

Acknowledgements

The author acknowledges many valuable contributions made by Dr. P. V. Lanspeary, Mr. C. Y. Wong and Mr. E. R. Hassan.

References

[1] Doligalski, T.L., Smith, C.R. & Walker, J.D.A., Vortex interactions with walls, Annual Review of Fluid Mechanics, **26**, 1994, 573-616.

[2] Hill, S.J., Nathan, G.J. & Luxton, R.E., Precession in axisymmetric confined jets, Proceedings of the 12th Australasian Fluid Mechanics Conference, Sydney, 1995.

[3] Kelso, R.M., On the mechanism of jet precession, Internal Report, Department of Mechanical Engineering, Adelaide University, 2001.

[4] Nathan, G.J., Hill, S.J & Luxton, R.E., An axisymmetric 'fluidic' nozzle to generate jet precession, Journal of Fluid Mechanics, **370**, 1998, 347-380.

[5] Nathan, G.J., The enhanced mixing burner, Ph.D. Thesis, Department of Mechanical Engineering, University of Adelaide, 1988.

[6] Perry, A.E. & Chong, M.S., A description of eddying motions and flow patterns using critical-point concepts, Annual Review of Fluid Mechanics, **19**, 1987, 125-155.

[7] Wong, C.Y., Lanspeary, P.V., Nathan, G.J, Kelso, R.M. & O'Doherty, T., Phase averaged velocity field within a fluidic precessing jet nozzle, Proceedings of the 14th Australasian Fluid Mechanics Conf., Adelaide, 2001.